Journal of Systems Engineering and Electronics
Vol. 28, No. 6, December 2017, pp.1089 – 1097

Method to reconnoiter pulse amplitude train for phased array radar based on Hausdorff distance

Chuan Sheng*, Yongshun Zhang, Wenlong Lu, and Junwei Xie

Air and Missile Defense College, Air Force Engineering University, Xi'an 710051, China

Abstract: This paper presents a method to estimate beam pointing of phased array radar by the pulse amplitude train, which is significant in radar electronic reconnaissance and electronic support measure. Firstly, the antenna patterns modeling of the phased array system is exploited to build the radar sweeping model and the signal propagation model. Secondly, the relationship between the variation of the radiated power and the antenna beam pointing angles in the given airspace is analyzed. Based on the above two points, the sample with obvious amplitude characteristics of the pulse amplitude train can be screened out after detecting the train peaks. Finally, the sample is matched to the subsequent pulse amplitude train based on the Hausdorff distance. The proposed methods have less prior knowledge and higher efficiency and are easier to process. By cross correlating the sample of the pulse amplitude train with the sample data of the antenna follow-up radiation, the probability of detection of the beam pointing direction becomes larger in case that the subsequent antenna beam returns to the specific position.

Keywords: beam pointing estimation, antenna pattern, pulse amplitude train, Hausdorff distance.

DOI: 10.21629/JSEE.2017.06.07

1. Introduction

Phased array radar can switch the beam direction rapidly by disposing the phase shifter with a wave controller. When compared to the mechanical scanning antenna, the phase array radar can overcome the capability limitation caused by the beam's rotating inertia. Besides, the characteristic of low probability of interception can be obtained due to the high agility of the beam, which presents new challenges to conventional reconnaissance [1]. The pulse description word (PDW), which contains the time of arrival (TOA), direction of arrival (DOA), pulse repetition frequency (PRF), radio frequency (RF) and pulse amplitude (PA), is used to sort the pulse and localize the position of radiation when a long-range radar reconnaissance is conducted [2 – 6]. Constrained by the operating range and deviation of the aircraft, the pulse amplitude train (PAT) cannot be easily obtained through the traditional method, so the information of pulse amplitude can only be used for trigger detection and few conferences focus on its extraction. Liao et al. established an emitter database based on prior knowledge and related model techniques to realize signal classification [7]. Quan et al. analyzed the scanning characteristic of phase array radar and proposed a pattern recognition method based on the rough sets theory to distinguish the signals from different radars [8].

As the received pulse train is dependent not only on transmitting antennas but also on receiving antennas [9, 10], pulse amplitude information is closely related to beam pointing, scanning mode and working state. As a part of the radar signature [11], the radar pulse amplitude train not only reflects the information of antenna radiation patterns but also has close relationship with the beam direction. For a particular phased system, the beam pattern varies with its direction, but it can be confirmed when the beam points at a fixed orientation. The transmitting power at a certain point in space changes with the radar beam direction. In radar searching mode, by modeling and simulating on the power distribution variation and analyzing the power variation rule at a given point in space, we can figure out the beam direction effectively.

Substantial attention has been paid to study the further application of PAT in recent years. The direction of mainlobe is estimated by the match of the sidelobe based on Hausdorff distance in [12], but the amount of prior information is required. The cycle binary algorithm was proposed to discriminate the whole waveform in [13], but the direction of main beam pointing cannot be extracted. In this paper, a method based on order-statistic filter (OSF) and Hausdorff distance is proposed to realize the main beam pointing recognition, with less dependence on prior knowledge, signal to noise ratio (SNR) and resolution.

Manuscript received March 17, 2016.
*Corresponding author.
This work was supported by the National Natural Science Foundation of China (61501501).

2. Modeling on transmission power over beam scanning

The transmitting power of phased array radar in space depends on its antenna pattern, the power of the transmitter and the slope distance between the fixed point and the radar. The power distribution is closely related to the searching modes of the radar in a certain space.

2.1 Antenna pattern function

The phased array radar changes the direction of beam steering through the changing of the phase offset in phase shifter. According to the antenna theory [14], the antenna pattern of the phased array is expressed as

$$G(\theta,\varphi)=D(\theta,\varphi)\cdot|F_a(\theta,\varphi)|\cdot|f(\theta,\varphi)|,$$
$$\theta\in\left[-\frac{\pi}{2},\frac{\pi}{2}\right],\quad \varphi\in[-\pi,\pi] \tag{1}$$

where $D(\theta,\varphi)$ is the pattern factor, $F_a(\theta,\varphi)$ is the array factor, and $f(\theta,\varphi)$ is the array element factor. θ and φ are the array elevation and azimuth angles under spherical coordinate set, respectively. $f(\theta,\varphi)$ is decided by the attributes of the antenna elements which are assumed to be cosine antenna elements working between 5 – 6 GHz. It can be expressed as follows:

$$f(\theta,\varphi)=\cos^m\theta\cos^n\varphi \tag{2}$$

where m and n are the cosine antenna exponents with their real numbers greater than or equal to 1. In the following sections, both m and n are chosen as 3.

When the beam points to direction (θ_0,φ_0), the pattern factor $D(\theta_0,\varphi_0)$ can be expressed as

$$D(\theta_0,\varphi_0)=$$
$$\left[\frac{4\pi A\eta}{\lambda^2}\cdot(1-|\varGamma(\theta_0,\varphi_0)|^2-L_\Omega)\cdot\cos\theta_0\right]^{\frac{1}{2}} \tag{3}$$

where A is the antenna aperture area. η is the aperture efficiency with amplitude weighting. λ is the wavelength of the corresponding working frequency. θ_0 is the angle from the antenna beam direction to the array normal direction. $|\varGamma(\theta_0,\varphi_0)|$ is the antenna mismatch coefficient. L_Ω is the insertion loss of the beam forming network.

In this simulation, suppose both η and $1-|\varGamma(\theta_0,\varphi_0)|^2-L_\Omega$ are equal to 1 in ideal conditions while in real phased array system they usually fall into the range between 0.4 – 0.7 and 0.6 – 0.8 respectively. As shown in (1) and (3), the pattern factor $D(\theta,\varphi)$ affects only the antenna magnitude while the beam/antenna shape is totally decided by the array factor $F_a(\theta,\varphi)$. For a planar rectangular array consisting of $(2N_x+1)\times(2N_y+1)$ antenna elements, distance between adjacent array elements is supposed to be $\mathrm{d}x$ in x axis and $\mathrm{d}y$ in y axis. The coordinate origin is located at (0,0) element. The array factor of planar array can be expressed as

$$F_a(\theta,\varphi)=\sum_{m=-N_x}^{N_x}\sum_{n=-N_y}^{N_y}I_{mn}\exp(\mathrm{j}k(m\mathrm{d}x\tau_x+n\mathrm{d}y\tau_y)) \tag{4}$$

$$\tau_x=\sin\theta\cos\varphi-\sin\theta_0\cos\varphi_0 \tag{5}$$

$$\tau_y=\sin\theta\sin\varphi-\sin\theta_0\sin\varphi_0 \tag{6}$$

$$k=\frac{2\pi}{\lambda} \tag{7}$$

where (θ_0,φ_0) is the beam steering, k is the number of beam positions, and I_{mn} is the weighting coefficient.

Consider a rectangular array consisting of 100×100 cosine antenna elements. The 3D response patterns of the array when the azimuth beam points to the (0°, 0°) and (45°, 45°) are shown in Fig. 1 and Fig. 2.

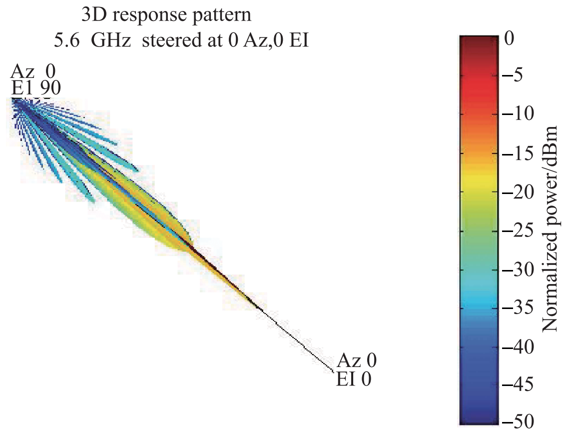

(a) 3-D antenna radiation pattern of rectangular array

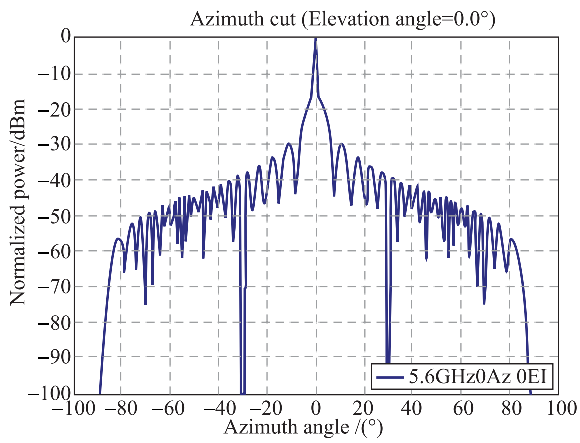

(b) Flat view of azimuth

Fig. 1 3D response pattern of the rectangular array when the azimuth beam points to (0°, 0°)

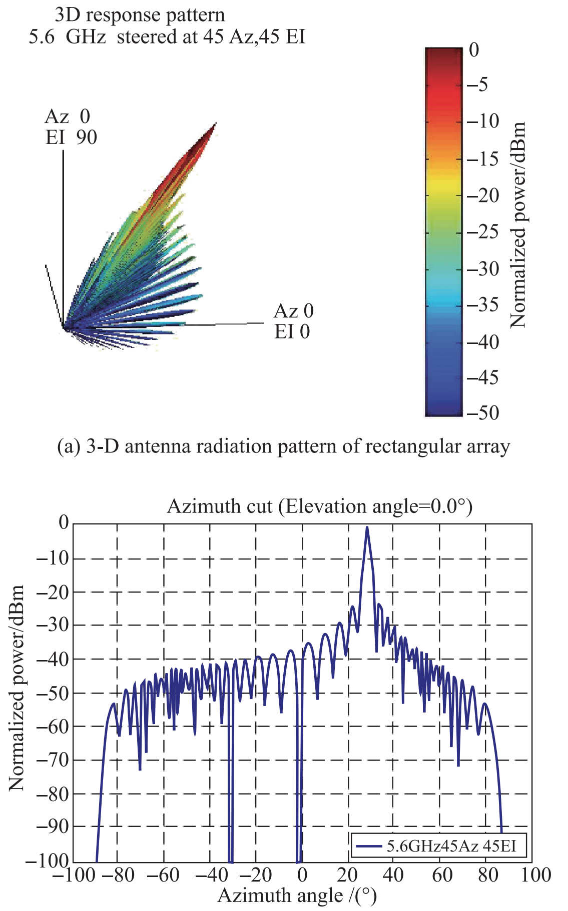

(a) 3-D antenna radiation pattern of rectangular array

(b) Flat view of azimuth

Fig. 2 3D response pattern of the array when the azimuth beam points to (45°, 45°)

Fig. 1 and Fig. 2 show that the antenna pattern of the array moves with the changing of the beam direction, which corresponds to (1). The pattern shapes under any beam direction can be safely affirmed when the antenna elements and structure of the array is assured.

2.2 Scanning models of the array beam

The scanning model of the array is used to describe how the beam direction angle changes with time when the array is searching for targets in the airspace [15,16]. According to different tasks, radars achieve optimal search and detection [17] with different scanning strategies such as linear scanning, elliptical scanning and multipoint scanning.

In air defense, the phased array radar systems usually perform searching tasks with the help of the target indication radar. After detecting targets in the specific airspace, the systems perform the task of target recognition and tracking. In order to obtain the variation of its scanning angles, the phased array beam scanning models should be analyzed, no matter whether there is target indication information or not and whether a target is found or not [18].

Fast switch of the wave beam is an important technique characteristic of phased-array radar which can not only track multi-batch targets, but also keep airspace search and surveillance when the tracking task is carried out. The rate of working data can directly influence the tracking accuracy of the guidance radar. Generally, the data rate is 10 Hz when accurate tracking is implemented while the data rate is 1 Hz when coarse tracking is implemented. Radar performs the task planning through the requirements towards different targets [19]. In this paper, the task planning of radar is set as follows:

k tasks, including one searching task and $k-1$ tracking tasks, are carried out by phase array radar. The corresponding time interval is $T_1, T_2, T_3, \dots, T_k$ and the data rate of tracking tasks is $s_1, s_2, s_3, \dots, s_{k-1}$, the time interval between the same tasks is the integral multiple of the dwell time of the wave beam, which can be expressed as T. The time interval of each task is set as follows:

$$T_i = N_i T, \quad i = 1, 2, \dots, k. \tag{8}$$

Suppose that the phased-array radar has a searching task, an accurate tracking task and a coarse tracking task. The time interval of accurate tracking is T_1 and the time interval of coarse tracking is T_2.

The array beam applies column by column sector scanning with a beam width of 2°×2° in the airspace with its azimuth angle range varing [−40°, 40°] and elevation angle range varing [−30°, 30°]. The beam stays 5 ms at every beam position. The interval between beam positions is $\Delta\alpha = 1°, \Delta\beta = 1°$. T_1 is 100 ms and T_2 is 1 s. The time series under different states can be shown in Fig. 3.

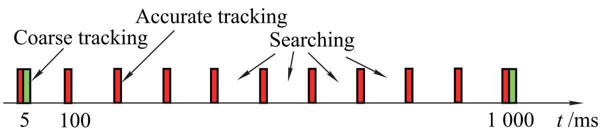

Fig. 3 Relationship between searching time and tracking time under two tracking states

Model the beam pointing of one sector's searching task. The corresponding beam pointing at the dwelling time when the searching task is implemented can be expressed as

$$\begin{cases} \alpha = \alpha_0 + \mathrm{mod}(n, A/\Delta\alpha), \quad n = 1, 2, \dots \\ \beta = \beta_0 + m\Delta\beta, \quad m = \mathrm{fix}[n/(A/\Delta\alpha)] \leqslant B/\Delta\beta \end{cases} \tag{9}$$

where B is the scanning range of the beam azimuth, A is the scanning range of the beam elevation, $\Delta\alpha$ and $\Delta\beta$ is the scanning step of the beam at elevation and azimuth respectively, (β, α) is the real-time pointing, (β_0, α_0) is its initial pointing, mod $(\cdot)$ is the modulus function and fix $(\cdot)$ is the integral function.

Two tracking tasks are inserted to searching tasks with time interval T_1 and T_2 according to Fig. 3 and (9). When the antenna finishes column by column scanning from left to right with a zigzag course on the vertical plane, the wave beam returns to the original point and begins the next sector searching. The searching time can be calculated as 25.4 s.

2.3 Signal propagation in space

To determine the exact transmitting power of the tested radar when its radiated power reaches the given positon in a space, the special characteristics of the radar space transmission are discussed.

Supposing the phased array radiates signal $x(t)$ to the airspace, the signal at distance R can be expressed [20] as follows:

$$y(t) = \frac{x(t-\tau)}{L} \tag{10}$$

where τ is the time delay, L is the signal attenuation in the process of propagation.

When the electromagnetic wave spreads at the light speed c, the time delay is

$$\tau = \frac{R}{c} \tag{11}$$

where R is the signal propagation range. Transmission attenuation coefficients in free space can be counted out with (12).

$$L = \frac{(4\pi R)^2}{\lambda^2} \tag{12}$$

where λ is the radar wavelength corresponding to its operating frequency.

Equations (10)−(12) build up the ideal signal propagation model in free space. In real cases, an atmospheric transmission loss of the radar signal occurs due to atmosphere refraction, atmospheric absorption, thermal noise and weather conditions such as cloud, rain, fog and snow.

In fact, it is quite difficult to describe these factors with accurate values. In general, these phenomena usually distribute uniformly in the earth aerosphere during a period of time and can be regarded as a loss factor in the radar equation [21]. Simultaneously, the loss factor is not a constant but a random variable obeying the Gaussian normal distribution. Thus the signal propagation model in actual airspace can be written as below:

$$y(t) = x\left(t - \frac{R}{c}\right)\frac{\lambda^2 \eta}{(4\pi R)^2} \tag{13}$$

where η is the loss factor of actual propagation in space.

Mitchell elaborated the relationship between power loss and propagation range during the actual transmission of electromagnetic wave in the atmosphere [22]. As is seen from the results, signal attenuation is in linear relationship with the propagation range at close quarters (within 50 miles), and the loss factor increases with the operating frequency.

3. Simulation of power variation at a fixed space point

When the phased array radar is scanning a given airspace, the antenna beam continuously scans a fixed area with its main lobes or side lobes, resulting in power variation. For a specified space point, as its relative positional relationship with radar is decided, it is not difficult to work out how their positional relationship affects the radiating power of the radar at this point while the radar is searching.

The position of one space point can be denoted with its coordinates in the phased array coordinate system. β, φ, and R represent the azimuth angle, elevation angle and distance of this point respectively [23]. Suppose that the radar power remains constant at each transmission. When the power is calculated, noise influence of the transmitter should be considered as well as man-made interference including industry disturbing, neighboring friend radar's interfering and enemy's intended jamming. Therefore, the actual power at a given space point is the summation of theoretical power and noise power. Noise power can be expressed with SNR and its value approximately obeys the normal distribution.

Model and simulation work are conducted with phased array system toolbox of MATLAB. Objects created in the toolbox contain antenna element, antenna array, transmitter, radiator and free space. Meanwhile, the noise model is added with the self-defined function. In the following simulations, the beam pointing angles are continuously converted into the array steering vector, then the simulated signals are radiated to the space point and the power of the specified space point is calculated. The parameters in simulation are shown in Table 1 and Table 2.

Table 1 Basic parameter settings

Parameter	Value
Array configuration	Rectangular
Array element number	100×100
Transmitter power /W	5×10^3
Radar working wavelength /cm	10
Emitting antenna gain /dB	40
Beam dwell time /ms	5
Beam width /(°)	2×2
Beam step /(°)	1
Receiving antenna gain /dB	20
Receiver SNR /dB	60
Receiver sensitivity /dBm	−100
The fixed space point	(30°, 20°, 30 000)

Table 2 Parameters of target moving model

Parameter	Target 1	Target 2
Tracking characteristics	Accurate	Coarse
Flight attributes	Uniform	Uniform
Track starting point	(0°, 0°)	(−20°, 0°)
Speed /(m/s)	150	200
Altitude /m	1 000	3 000

The SNR in the receiver [24] can be expressed as

$$\mathrm{SNR} = 10\lg(P_s/P_n) \tag{14}$$

where P_s is the total energy of PAT and P_n is the energy of noise. The power of signal in the receiver can be expressed as

$$P_s = \frac{P_t G_t G_r \lambda^2}{(4\pi R)^2} \tag{15}$$

where P_t denotes the emitting power of radar, G_t denotes the gain of the radar antenna, G_r denotes the antenna gain of the reconnaissance plane, λ denotes the wave length and R denotes the distance between the reconnaissance plane and the radar.

Choose $P_n = S_{min} = -100$ dBm according to Table 1 and Table 2, then the SNR of mainlobe can be calculated as 135 dB and the SNR of the fifth sidelobe is 70 dB. When the slope distance of the specific point is set as 60 km, the SNR of mainlobe as well as the fifth sidelobe can be 129 dB and 64 dB, so the SNR in the simulation would be set as 60 dB. Fig. 4 shows the changing of the normalized energy in the specific point when two tracking tasks are implemented at the same time.

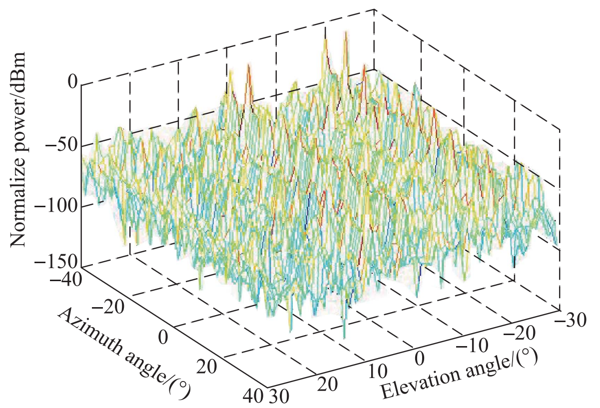

Fig. 4 Relationship between the antenna sweeping angle and the power of the given point

Fig. 5 shows the power variation at the point (30°, 20°, 30 000) when the phased system is searching in space according to the one searching task and two tracking tasks. As can be seen from Fig. 4 and Fig. 5, power variation at this point partly reflects the antenna scanning principle, which is listed as follows:

(i) The peak of the amplitude value occurs periodically due to the fact that the antenna's main lobes cyclically get close to the point in elevation;

(ii) Power envelop firstly increases and then decreases along with the main lobes gradually approaching and deviating from the point in azimuth;

(iii) Transmitting power acquires its maximum value when the antenna beam is directing at this point;

(iv) The tracking task presents periodic pulse spikes in the pulse amplitude train.

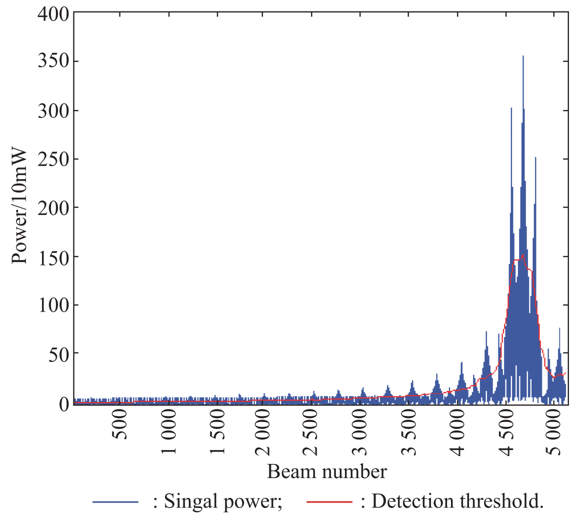

Fig. 5 Power variation curve at the given point along with time

4. Analysis of the antenna beam direction

4.1 Pulse amplitude train samples selection

In accordance with the results in Fig. 5, the antenna beam direction is analyzed to find the moment when the main lobe peak values and side lobe peak values traverse to the receiving point, and extract a fixed number of radiation samples around this point.

The sample in Fig. 5 is preprocessed with the OSF method. In the figure, the train of length reaches 5 076 points, where a full traversal of peak values covers around 240 points. The number N of sliding window group x is assumed to be 256 points, and then the threshold Z of OSF on the samples train is calculated.

x_i $(i = 1, 2, \ldots, 256)$ is arranged in ascending rank order to be x'_j. Assume that

$$Z = x'_k. \tag{16}$$

Assume $k = 3N/4$ (i.e., $k = 192$) as the noise level of the antenna active radiating samples is much lower than targets scattering echo.

Fig. 6 shows the testing results with the OSF method. It can be obviously shown that the super threshold samples reserve all the peak values which are formed during the traversal of the main lobe and side lobe peaks in Fig. 5. The nonzero super threshold sampling points $M_{\max}$ in the peak value region shrinks to less than 50 points. Suppose that the amount of super threshold sample groups is $a(m)$, the envelope center of gravity can be calculated as follows:

$$\sum_{m=0}^{N} a(m) = \frac{1}{L_s}\sum_{i=0}^{N}(\sum_{m=0}^{i} a(m)) \tag{17}$$

where L_s is a constant value related to $M_{\max}$ which refers to the maximum number of signals among a group of super threshold signals. The principle of selecting $M_{\max}$ is: $L_s \geqslant M_{\max}/2$, so L_s equals 30. N is the intersection point of first integral and double integral. Solving N in (17), then the samples group envelop center of the gravity serial number can be obtained, which can be expressed as

$$N_{\text{peak}} = N - L_s. \tag{18}$$

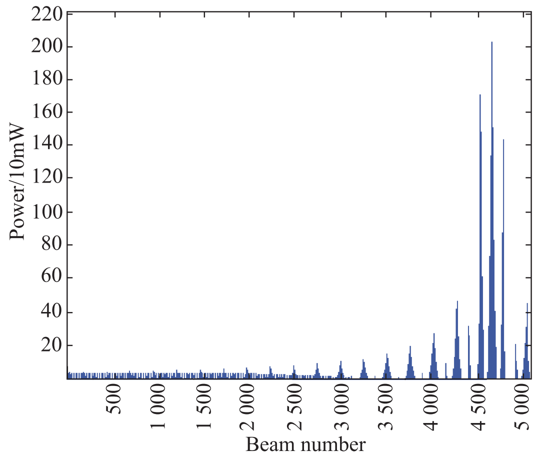

Fig. 6 Detection result with the OSF method

The calculated results of the the gravity center of each peak region is shown in Table 3.

Table 3 Detection results

Number	Peak/10mW	Beam number
1	6.011	81
2	6.581	206
3	7.035	459
4	6.699	721
5	8.078	967
6	9.378	1 475
7	10.17	1 729
8	11.08	1 983
9	12.17	2 237
10	13.49	2 491
11	15.14	2 745
12	17.28	2 998
13	20.17	3 253
14	24.35	3 507
15	31	3 760
16	43.3	4 015
17	74.19	4 269
18	72.87	4 395
19	303.1	4 523
20	357	4 648
21	252.7	4 774
22	77.69	5 029

As shown in Table 3, the pulse peak generated by the tracking task is filtered when the double integral method is used to detect the peak value.

4.2 Radar beam direction identification

In order to increase the probability of beam direction identification, the detected power peaks in Table 3 is first rearranged based on the altitude value, then, certain sample data before and after the peak value points are taken as the matching samples. Finally, the subsequently received radiation data are matched to acquire real-time beam direction information using the Hausdorff distance curve matching method.

Step 1 The extraction of peak value sample curve

As depicted in Fig. 7, the 19th and 20th points, which own the biggest peak value amplitude in Table 3, are taken as an example, 128 points before and after the peak value point is taken as a curve sample.

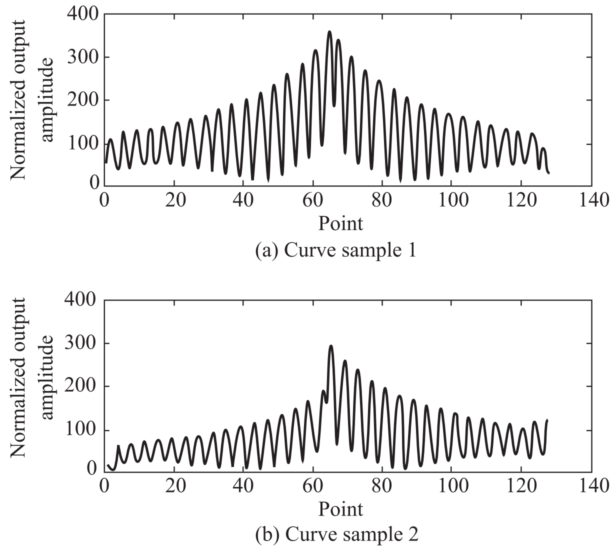

Fig. 7 Peak value sample curve

Step 2 Calculate the curvature set $\boldsymbol{A}$ of the sample curve

Any curvature of the curves can be calculated by

$$\kappa = \frac{y''}{(1 + y'^2)^{3/2}}. \tag{19}$$

The calculated curvature result of the sample in Fig. 7 is shown in Fig. 8. The curvature set of the curvature sample 1 – 2 can be defined as

$$\boldsymbol{A}^i = \{a_1^i, a_2^i, \dots, a_{128}^i\}, \quad i = 1, 2.$$

Step 3 Calculate Hausdorff Distance for amplitude data using the searching method of 128 points sliding window

Hausdorff Distance is the biggest/smallest distance defined in two points set [25], which is mainly used to measure the matching degree of the two points set. The Hausdorff Distance between the finite point set $\boldsymbol{A} = \{a_1, a_2, \ldots, a_p\}$ and $\boldsymbol{B} = \{b_1, b_2, \ldots, b_p\}$, can be defined as

$$H(\boldsymbol{A}, \boldsymbol{B}) = \max(h(\boldsymbol{A}, \boldsymbol{B}), h(\boldsymbol{A}, \boldsymbol{B})) \qquad (20)$$

where $h(\boldsymbol{A}, \boldsymbol{B}) = \max\min \|a - b\|$, $h(\boldsymbol{B}, \boldsymbol{A}) = \max\min \|b - a\|$, $\| \cdot \|$ is the distance pattern defined in points sets $\boldsymbol{A}$ and $\boldsymbol{B}$. L_2-pattern is Euclidean Distance.

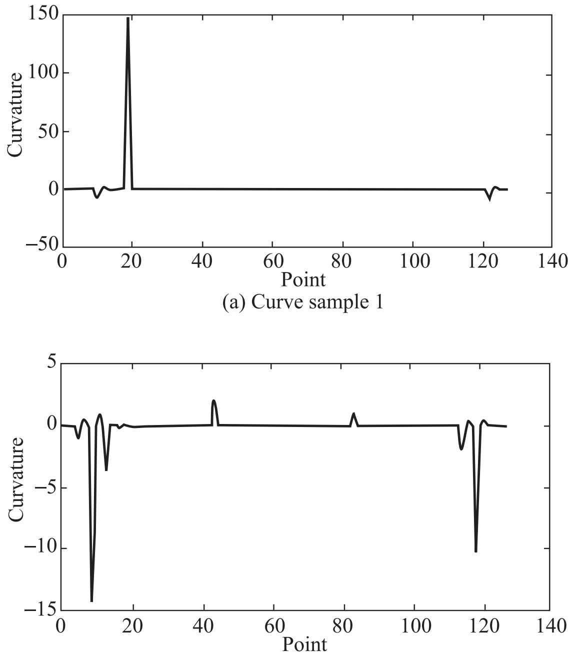

(a) Curve sample 1

(b) Curve sample 2

Fig. 8 Peak value sample curve curvature

In simulation, it can be assumed that the subsequent received radar radiation data begin from 10 s (that is 500 point) in Fig. 5, in which disturbing noise (SNR = 60 dB) is added. Pick up curve sampling of the subsequent received radar radiation data using 128 points sliding window, and calculate the curvature set $\boldsymbol{B}^j = \{b_1^j, b_2^j, \ldots, b_{128}^j\}$, in which j refers to the subsequent sampling numbers, $j = 500, 501, \ldots, 5\ 076$. As shown in Fig. 9, the Hausdorff Distance curve composed of the sampling points can be acquired from (20). It can be seen in Fig. 9 that Hausdorff Distance Zero (the curve sample 1: 0.003 268, the curve sample 2: 0.002 138) appears when radar subsequent beams scan the curve sample 1 (beam number: 4 648) and the curve sample 2 (beam number: 4 523). In test, according to the simulation results, pick up the proper matching threshold $e = 1$. When $H(\boldsymbol{A}, \boldsymbol{B}) < e$, the sample curve can be judged to match to the radar radiation curve.

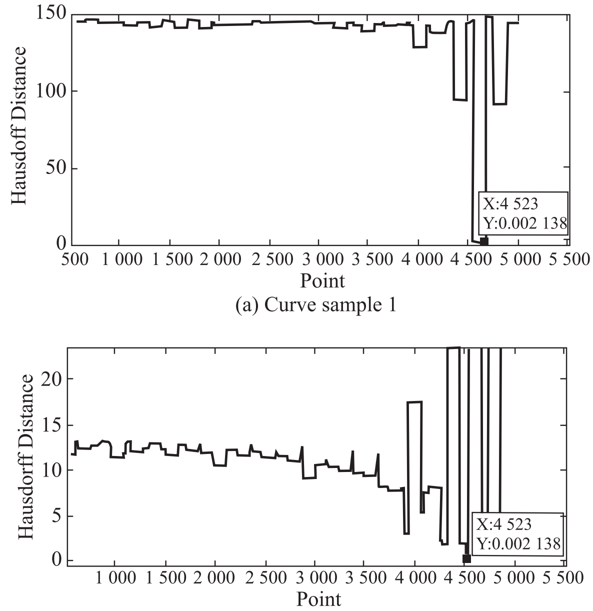

(a) Curve sample 1

(b) Curve sample 2

Fig. 9 Hausdorff Distance curve

4.3 Performance analysis

Consider the simulation time is 100 and $e = 1$. Both the detection probability and false alarm probability are counted to show the performance of the algorithm under different SNRs and sliding window widths.

Table 4 shows that the algorithm has a better performance when the SNR is higher. The detection probability is 91% when SNR is 30 dB, which can increase to 99% when SNR is 35 dB.

Table 4 Detection result with noise (e = 1, Points = 128)

Probability	SNR /dB			
	25	30	35	60
Detection probability /%	2	91	99	100
False alarm probability/%	0.30	0.29	0.24	0.01

Table 5 shows that the detection performance would be the best when the sliding window width is equal to the peak beam width. The false alarm probability is on the rise when the sliding window width is bigger, which results from the decrease of the uniqueness of PAT. The condition would be the same when the sliding window width is narrower, due to the decrease of resolution of PAT. Besides, the computation of the proposed method has a square relationship with the sliding window width.

Table 5 Detection results with different sampling points (e = 1, SNR = 35 dB)

Probability	Point		
	64	128	256
Detection probability/%	100	99	100
False alarm probability/%	3.8	0.24	4.7

5. Conclusions

In this paper, a method based on OSF detection and Hausdorff Distance is proposed to extract the information of PAT in a fixed point, which can be used for beam pointing recognition of the main beam. When the jamming equipment releases the sidelobe track deception jamming signal, the proposed method can significantly improve the probability of being triggered and tracked, besides, it can largely decrease the hardware sizing.

In the arithmetic, the pulse amplitude train sample for specific coordinate points in space can be picked up through phased-array radar beams modeling.

In the arithmetic, the OSF method can filter the train sample and find out the distinct corner of the train sample curve quickly.

Only curve shape needs to be matched so less computation is conducted in the proposed method. Additionally, it is not sensitive to the radar transmitting power and SNR which is beneficial to reduce the difficulties in hardware sampling channel design.

References

[1] R. G. Wiley. *ELINT: The interception and analysis of radar signals*. Boston: Artech House, 2006.
[2] Q. Guo, P. L. Nan, X. Y. Zhang, et al. Recognition of radar emitter signals based on SVD and AF main ridge slice. *Journal of Communication and Networks*, 2015, 17(5): 491 – 498.
[3] F. Li, L. X. Ren, J. Cao, et al. Short pulse groups searching based on isomorphic sequences. *Electronics Letters*, 2014, 50(24): 1875 – 1877.
[4] L. Q. Li, H. B. Ji, L. Jiang. Quadratic time-frequency analysis and sequential recognition for specific emitter identification. *IET Signal Processing*, 2011, 5(6): 568 – 574.
[5] L. Jiang, L. Li, G. Q. Zhao. Polyphase coded low probability of intercept signals detection and estimation using time-frequency rate distribution. *IET Signal Processing*, 2016, 10(1): 46 – 54.
[6] D. Zeng, X. Zeng, H. Cheng, et al. Automatic modulation classification of radar signals using the Rihaczek distribution and Hough transform. *IET Radar, Sonar & Navigation*, 2012, 6(5): 322 – 331.
[7] Y. P. Liao, S. C. Zhou, T. Shu. A study on radar emitter recognition technology using individual characteristics. *Modern Radar*, 2015, 37(3): 36 – 41. (in Chinese)
[8] W. Quan, P. Li, F. K. Xu. An algorithm of signal sorting and recognition of phased array radars. *Proc. of the IEEE International Conference on Signal Processing*, 2010: 1877 – 1880.
[9] M. Dudek, I. Nasr, G. Bozsik, et al. System analysis of a phased-array radar applying adaptive beam-control for future automotive safety applications. *IEEE Trans. on Vehicular Technology*, 2015, 64(1): 34 – 47.
[10] D. S. Jang, H. L. Choi, J. E. Roh. Optimization of surveillance beam parameters for phased array radars. *Proc. of the IET International Conference on Radar Systems*, 2012: 1 – 5.
[11] J. Matuszewski. The radar signature in recognition system database. *Proc. of the International Conference on Microwave Radar & Wireless Communications*, 2012: 617 – 622.
[12] X. Li, C. Y. Wang, Q. Wang. The method to reconnoiter the main beam direction of phased array radar based on the side beam surveying. *Journal of China Academy of Electronics and Information Technology*, 2013, 8(5): 507 – 511. (in Chinese)
[13] S. Ma, Z. Liu, W. L. Jiang. A method for multifunction radar pulse train analysis based on amplitude change point detection. *Acta Electronica Sinica*, 2016, 41(7): 1436 – 1441. (in Chinese)
[14] G. Y. Wang, L. D. Wang. *Mathematical simulation and evaluation of radar EW system*. Beijing: National Defense Industry Press, 2004. (in Chinese)
[15] S. J. Tang, D. Y. Bi, Y. S. Xu, et al. The searching model and strategy for passive sensor cue of phased array radar. *Proc. of the International Conference on Mechanical and Electronics Engineering*, 2015, 07003: 1 – 5.
[16] T. Robertazzi. Scheduling beams with different priorities on a military surveillance radar. *IEEE Trans. on Aerospace and Electronic Systems*, 2012, 48(2): 1725 – 1739.
[17] D. J. Matthiesen. Efficient beam scanning, energy allocation, and time allocation or search and detection. *Proc. of the IEEE International Symposium on Phased Array Systems and Technology*, 2010: 361 – 368.
[18] D. S. Jang, H. L. Choi, J. E. Roh. Search optimization for minimum load under detection performance constraints in multifunction phased array radars. *Aerospace Science and Technology*, 2015, 40: 86 – 95.
[19] T. Robertazzi. Scheduling beams with different priorities on a military surveillance radar. *IEEE Trans. on Aerospace and Electronic Systems*, 2012, 48(2): 1725 – 1739.
[20] C. Amanda, D. William, R. Teryl, et al. Real-time, low-cost, due regard radar target simulation. *Proc. of the IEEE Radar Conference*, 2015: 728 – 733.
[21] MathWorks, United States. Phased array system toolboxTM user's guide. http://www.mathworks.com, 2014.
[22] R. L. Mitchell. *Radar signal simulation*. Norwood: Artech House, 1976.
[23] B. Svante, N. Anders, I. Mats, et al. Auxiliary beam terrain-scattered interference suppression: reflection system and radar performance. *IET Radar, Sonar & Navigation*. 2013, 7(8): 836 – 847.
[24] S. B. Wang, X. F. Chen, Y. Wang, et al. Nonlinear squeezing time-frequency transform for weaksignal detection. *Signal Processing*, 2015, 113(C): 195 – 210.
[25] D. P. Huttenlocker, G. A. Klanderman. Comparing images using the Hausdorff distance. *IEEE Trans. on Pattern Analysis and Machine Intelligence*, 1993, 15(9): 850 – 863.

Biographies

Chuan Sheng was born in 1979. He received his M.S. degree from the Air Force Engineering University in 2006 and is now studying for his Ph.D. degree in the same university. He is currently an associate professor in Air Force Engineering University. His research interests are electronic jamming and anti-jamming and radar environment simulation.
E-mail: hidaicy@126.com

Yongshun Zhang was born in 1961. He received his M.S. degree from Catholic University of Louvain, The Kingdom of Belgium, in 1994, and Ph.D. degree from Xidian University, Xi'an, China, in 2011. He currently is a professor in Air Force Engineering University. His research interests are space-time adaptive processing, radar signal processing and high-resolution ISAR imaging.
E-mail: zysgcdx@sina.com

Wenlong Lu was born in 1988. He received his M.S. degree from Air Force Engineering University in 2010 and is now studying for his Ph.D. degree in the same university. His research interests include electronic war (EW) techniques based on stealth platform and microelectronic techniques applying to EW systems.
E-mail: youranqixia521@126.com

Junwei Xie was born in 1970. He received his Ph.D. degree from Air Force Engineering University. Currently he is working in Air Force Engineering University as a professor. His research interests include electronic jamming and anti-jamming and radar environment simulation.
E-mail: jun_wei_xie@126.com